catalysts

MDPI

Article

Glycerol Dehydration to Acrolein over Supported Vanadyl Orthophosphates Catalysts

Giovanna Ruoppolo [1], Gianluca Landi [1,*] and Almerinda Di Benedetto [2]

[1] Institute for Researches on Combustion—CNR P.le Tecchio 80, 80125 Naples, Italy; ruoppolo@irc.cnr.it
[2] Dipartimento di Ingegneria Chimica, dei Materiali e della Produzione Industriale, University of Naples Federico II, P.le Tecchio 80, 80125 Naples, Italy; almerinda.dibenedetto@unina.it
* Correspondence: gianluca.landi@cnr.it; Tel.: +39-08-1768-2235

Received: 21 May 2020; Accepted: 11 June 2020; Published: 15 June 2020

Abstract: Biodiesel has been identified as one of the notable options for at least complementing conventional fuels. From a transesterification reaction, crude glycerol is produced as the main by-product. Given the difficultly in upgrading to high-grade glycerin and glycerol market saturation, alternative routes to more value-added products have aroused significant interest. In this work, we proposed supported vanadyl orthophosphates (VOP) as catalysts for the glycerol dehydration to acrolein. VOP supported on γ-Al_2O_3, TiO_2, and ZrO_2 were prepared, characterized by inductively coupled plasma mass spectrometry (ICP-MS), X-ray diffraction (XRD), N_2 physisorption and temperature-programmed desorption of ammonia (NH_3-TPD), and tested under different operating conditions. All the samples showed low coke formation in the presence of molecular oxygen in the feed. Acrolein is the main condensable product, with carbon balance being satisfactory under most operating conditions. VOP supported onto alumina provided the best catalytic performance, due to a good balance between the acid (weak and medium acid sites) and redox sites, thereby appearing as a good candidate for glycerol dehydration to acrolein.

Keywords: glycerol; acrolein; vanadyl orthophosphate; alumina; titania; zirconia; biodiesel

1. Introduction

Biodiesel has been identified as a notable option for complementing conventional fuels. Its production is from renewable biological sources, mainly vegetable oils (rape, soybean, palm) and an alcohol (usually methanol) used to break down fatty acids from glycerol via a transesterification reaction, according to the reaction reported in Figure 1.

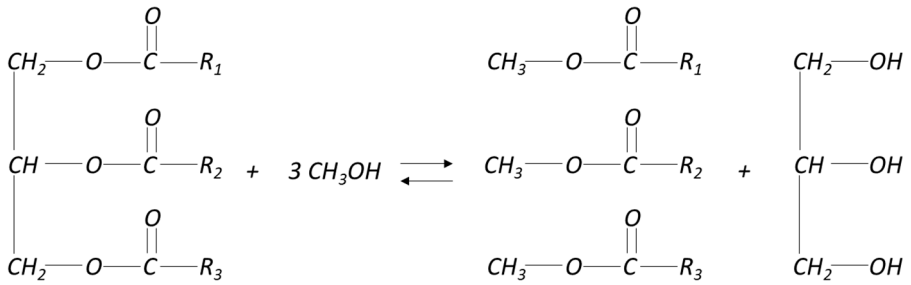

Figure 1. Transesterification reaction of fatty acids for the production of biodiesel. (R_1, R_2, and R_3 are hydrocarbons chains containing 15–21 C atoms [1–4].)

Glycerol accounts for about 10 wt.% of the biodiesel produced [5]. Crude glycerol should be upgraded to obtain "technical grade" glycerol and, by a further purification, United States

Pharmacopeia (USP; appropriate for food and pharmaceutical products) and Food Chemicals Codex (FCC; appropriate for use in food) glycerin, both requiring ≈100% purity. However, the glycerol surplus together with its difficult upgrading in the presence of methanol [6] makes crude glycerol upgrading disadvantageous [7–9], especially if the price decrease of glycerol is considered [9–11].

For the above reasons, several alternative routes have been investigated to upgrade glycerol to more value-added products [6,7,11–23]. Among these routes, glycerol dehydration to acrolein has received significant interest due to the broad use of acrolein in the chemical industry. Acrolein is converted mainly to acrylic acid, but also acrylic acid esters, glutaraldehyde, methionine, polyurethanes, and polyester resins [24].

Several catalysts have been proposed for glycerol dehydration, including heteropolyacids, zeolites, metal oxides, mixed metal oxides, phosphates and pyrophosphates, and mixed systems thereof [5,18,25–46]. Given the vast number of reactions potentially occurring during glycerol dehydration, the proper choice of catalyst is paramount. A non-exhaustive reaction scheme is reported in Figure 2. This scheme has been derived from schemes suggested by Katryniok et al. [47] and Jiang et al. [48], and the references within. The occurrence of each reaction depends on the reaction conditions (temperature, oxidizing or reducing environment) and the catalytic active sites.

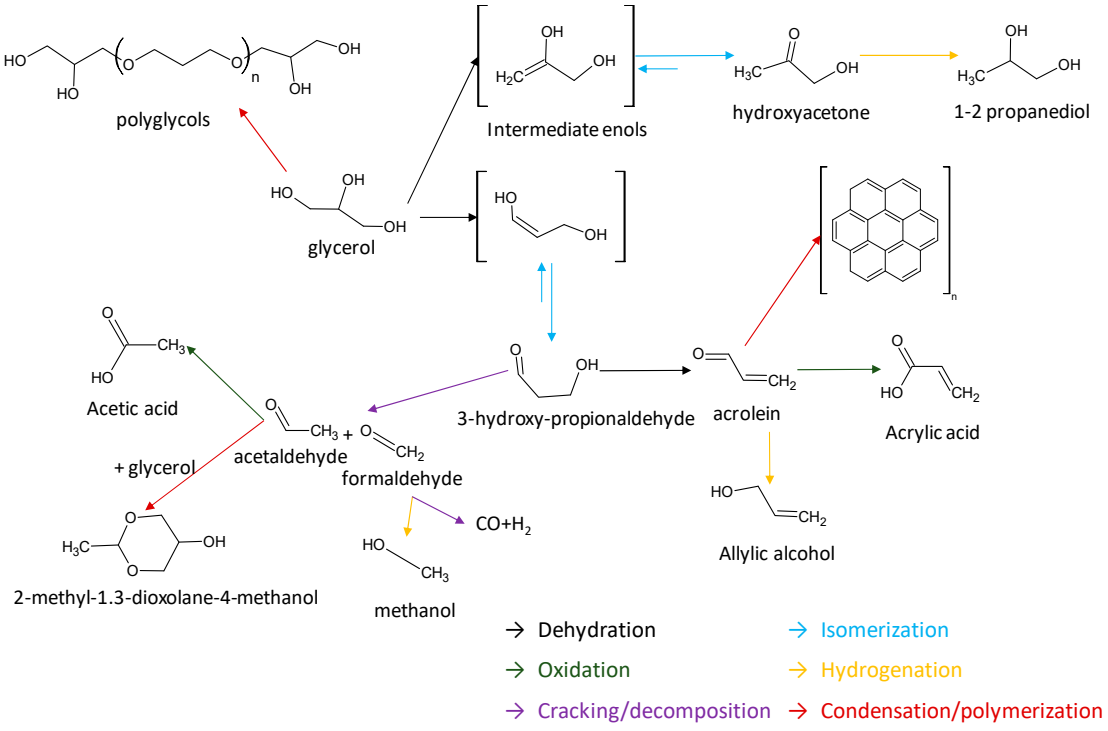

Figure 2. Reaction scheme of glycerol dehydration (derived from References [47,48]).

The key point for the development of catalysts is the balance of the acid sites. For instance, in H-ZSM5 based catalysts the co-presence of acid sites of different types (Lewis/Brønsted) and strength both improved the acrolein yield and decreased coke formation [5]. Coking is the major deactivating phenomenon, and it is still an open issue [48], despite several efforts to develop coking-resistant catalysts [49–51]. Coke is formed by cyclization, condensation, and polymerization reactions occurring on acid sites (see Figure 2). A strategy to reduce coking is to oxidize coke precursors by adding oxygen in the feed stream and by doping the catalyst with redox sites [48].

Vanadyl orthophosphates ($VOPO_4$) have been proposed for the oxidative dehydrogenation (ODH) of ethane and propane [52,53], and they both have acid and redox properties. In particular, $VOPO_4$ supported on γ-Al_2O_3, TiO_2, and ZrO_2 showed the best catalytic properties towards propane ODH due to good active phase dispersion and improved redox properties, the best catalyst being

the TiO_2-supported sample. In vanadyl phosphorus oxides [54–57], different vanadyl phosphate phases (mainly related to V^{4+} and V^{5+}, but also to V^{3+}) are typically detected in both as-prepared and used catalysts. In particular, V^{4+} species have been detected in vanadyl orthophosphates under reducing reaction conditions [58].

In this work, $VOPO_4$ supported on γ-Al_2O_3, TiO_2, and ZrO_2 were tested in the gas-phase glycerol dehydration. The catalyst performances were related to the site acid properties. Despite the possible co-presence of different vanadyl phosphates, in this work, the catalysts were labelled as VOP (vanadyl orthophosphate).

2. Results

2.1. Catalysts Characterization

Table 1 shows the specific surface areas (SSA) of the bare supports. Al_2O_3 has the largest surface area (190 $m^2 \cdot g^{-1}$), while the lowest exposed surface corresponds to ZrO_2 (49 $m^2 \cdot g^{-1}$). Accordingly, the active phase load corresponding to the monolayer was directly related to the SSA and steadily increased from 3.6 to 14.0 wt. %. After the VOP deposition, the samples showed SSA values close to the corresponding supports, suggesting a good dispersion of the active phase.

Table 1. Nominal vanadyl orthophosphate (VOP) content (wt. %), surface area ($m^2 \cdot g^{-1}$) of supports and catalysts, and H_2/V as calculated by the temperature-programmed reduction in hydrogen (H_2-TPR).

Catalyst	Nominal VOP Content	Support Surface Area	Catalyst Surface Area	H_2/V [a]
VOP/Ti	9.6	125	125	0.71
VOP/Al	14.0	190	183	0.67
VOP/Zr	3.6	49	43	1.07

[a] as reported by Casaletto et al. [53].

XRD spectra of both fresh and used samples (not reported) showed only the signals corresponding to the supports, and no peak due to vanadyl orthophosphate was detected, which was in agreement with previous results [53]. Thus, no VOP phase segregation occurs in these samples, suggesting a good active phase dispersion onto the support and no segregation phenomena occurring under the reaction conditions.

The results in terms of NH_3-TPD profiles and the quantitative analysis are shown in Figures 3 and 4, respectively. The profile shapes are similar, suggesting that the same acid sites are detectable on each sample. This also suggested the negligible contribution of the supports (characterized by very different acidity) to overall acidity of the samples. This agreed with the good dispersion of the active phase. However, it is worth noting that the interaction between the VOP and support strongly affects the active phase features [59]. As shown in Figures 3a and 4, VOP/Al is characterized by the largest amount of acid sites. This sample was characterized by the highest VOP amount, too. Figure 3b shows the desorbed ammonia per VOP weight. Profiles of VOP/Al and VOP/Ti were similar but they did not overlap. The zirconia supported sample showed a larger ammonia desorption per VOP amount. This could be addressed to the higher coordination between ammonia and the acid sites. However, due to the low VOP content, the uncertainty of the ICP analysis could be higher. Nevertheless, VOP/Zr showed the lowest catalytic activity (see Section 2.2.2), and thus, further investigations were not carried out.

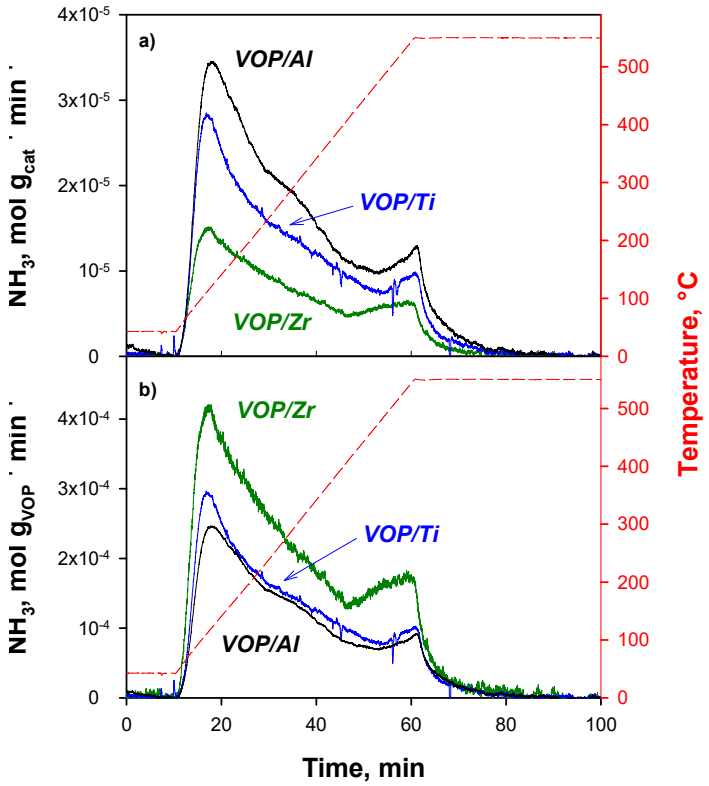

Figure 3. NH_3-TPD profiles of the VOP/x catalysts for the catalyst (**a**) and VOP weight (**b**).

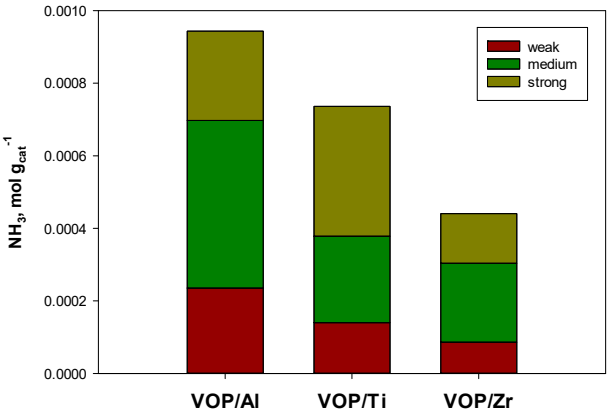

Figure 4. Overall and partial ammonia amounts desorbed from the VOP/x catalysts during NH_3-TPDs.

From the quantitative point of view (Figure 4), VOP/Al showed the most significant amounts of both weak and medium acid sites, while the highest amount of strong acid sites was detected in VOP/Ti. Acrolein formation has been related to the acid sites and, in particular, to the weak and the medium acidity [27,31,35,36,60,61]. It is worth noting that the strong acid sites can be related to the catalyst deactivation by coking [27,35,36,60,61].

Redox properties of the samples were previously studied [53], and the corresponding results are given in Table 1 as H_2/V. VOP/Al shows the lowest H_2/V ratio, suggesting that vanadium is less reducible. Conversely, the VOP/Zr sample was the most reducible.

2.2. Catalytic Activity

2.2.1. Effect of the Reaction Conditions

VOP/Ti showed the best catalytic properties towards propane oxidative dehydrogenation (ODH) [53], and thus, it was used as the reference catalyst to evaluate the effect of the reaction conditions on the catalytic performance.

The effect of the furnace temperature was investigated in the range 210–255 °C at a fixed contact time $\tau = 0.057$ g·s·cm^{-3} and feed composition Gly/H_2O/O_2/N_2 = 2/41/6/51 vol. %.

In Figure 5, the glycerol conversion (Figure 5a) and the yields of several products (Figure 5b–d) are shown as a function of temperature.

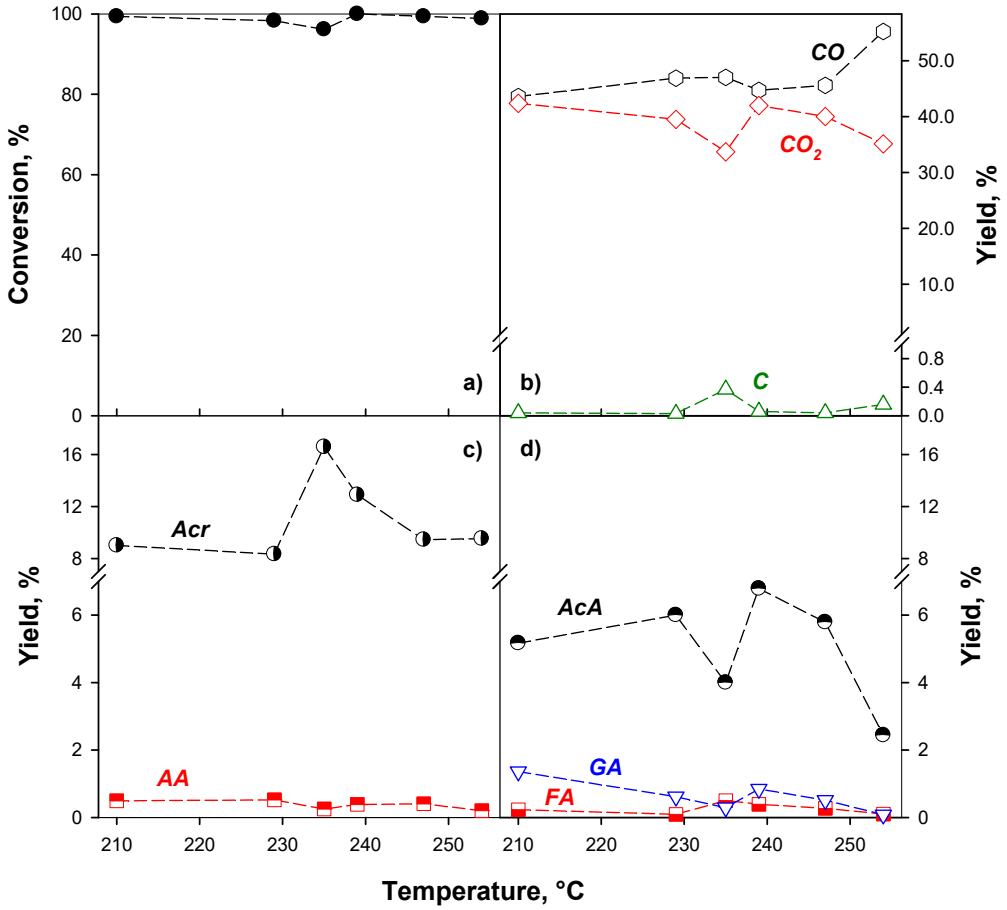

Figure 5. (**a**) Glycerol conversion, (**b**) yields to CO (⬡), CO_2 (◇), and coke (C, △), (**c**) yields to acrolein (Acr, ◑) and acrylic acid (AA, (⬒), (**d**) yields to acetic acid (AcA, ◓), formic acid (FA, ⬓), and glycolic acid (GA, ▽) as a function of the temperature on VOP/Ti; $\tau = 0.057$ g·s·cm^{-3}, Gly/H_2O/O_2/N_2 = 2/41/6/51 vol. %.

Glycerol conversion was high and quite complete in the whole temperature range investigated. Acrolein was the most abundant condensable product, while the acrylic acid yield was very low.

From these results, it appeared that in the presence of molecular oxygen, VOP was poorly active towards acrolein oxidation to acrylic acid or, more probably, too active towards acrylic acid oxidation. This behavior has been previously reported on vanadyl pyrophosphate [62]. The maximum yield (16%) has been obtained at 235 °C. Detected by-products included acetic acid, formic acid, and glycolic acid. Among these species, only the production of the acetic acid was significant, even if its highest yield was lower than 7% (Figure 5d). Coke formation was negligible (Figure 5b), due to the good oxidation properties of the VOP catalyst. As reported in Section 1, resistance to coking is a major issue

to be solved [48] and the intimate contact between the acid sites, related to phosphate, and the redox sites, related to vanadium, provides fast conversion of coke precursors into CO_x, which are the most abundant products (Figure 5b). CO increases at temperatures above 235 °C, while CO_2 slightly decreases; therefore, oxidation of acrolein and acetic acid (where the yields decrease by increasing the temperature above 235 °C) mainly produces carbon monoxide.

The effect of contact time on the catalytic properties is shown in Figure 6, at 230 °C. Glycerol conversion slightly increases by increasing the contact time. As expected, acrolein yield increased, while acrylic acid, acetic acid, and glycolic acid yields showed a maximum. In particular, the acetic acid yield dropped down to zero at the highest contact time. These results suggested that oxidation of acids to CO_x was significantly faster than acrolein oxidation, while acrolein formation was faster than its oxidation at this temperature. Coke formation was still negligible.

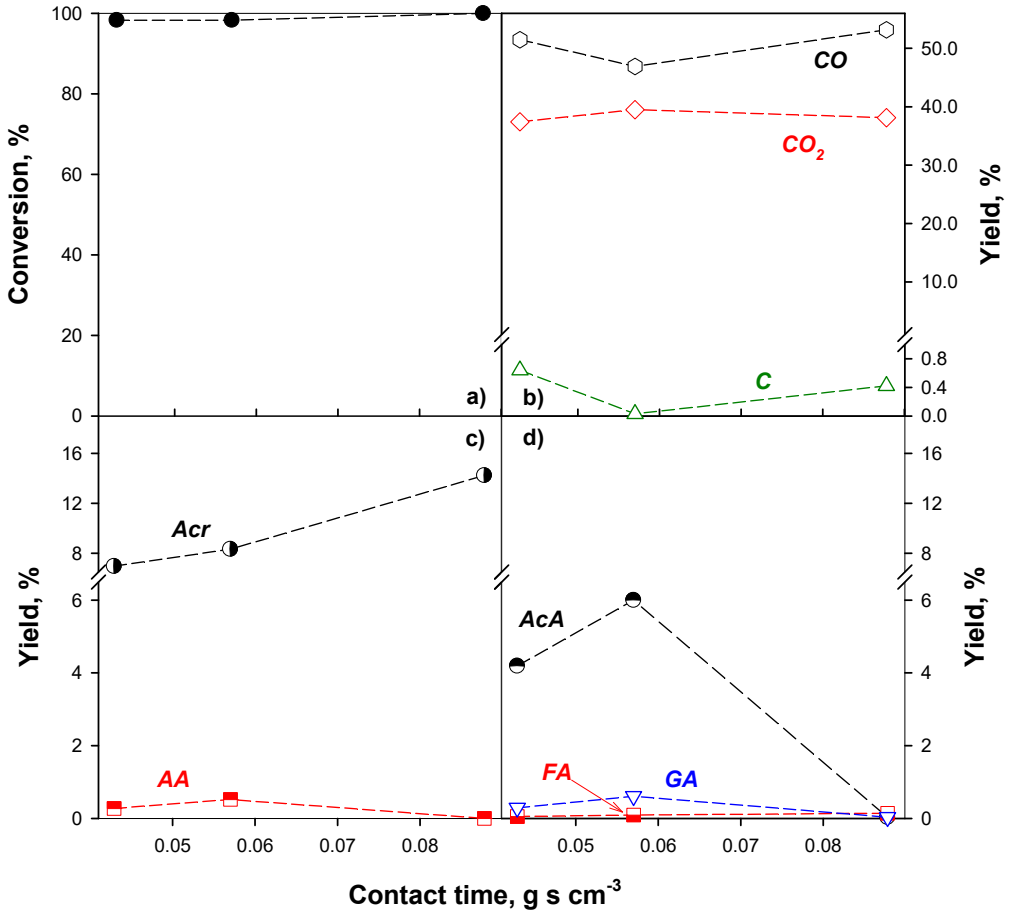

Figure 6. (**a**) Glycerol conversion, (**b**) yields to CO (○), CO_2 (◇), and coke (C, △), (**cr**) yields to acrolein (Acr, ◑) and acrylic acid (AA, (⬒), (**d**) yields to acetic acid (AcA, ◓), formic acid (FA, ⬓), and glycolic acid (GA, X) as a function of the contact time on VOP/Ti; temperature = 230 °C, $Gly/H_2O/O_2/N_2$ = 2/41/6/51 vol. %.

The combined effect of temperature and contact time on glycerol conversion and acrolein yield is shown in Figure 7. Independently from the contact time, temperatures higher than 200 °C were needed to get complete (or almost complete) conversion. Moreover, at low temperatures, incomplete carbon balance was obtained due to the formation of unknown products (not reported). The reaction temperatures providing the best acrolein production decreased. This behavior was less prominent for other products (not reported), but by decreasing the contact time from 0.088 $g{\cdot}s{\cdot}cm^{-3}$ to 0.043 $g{\cdot}s{\cdot}cm^{-3}$, the production peak shifted at higher temperatures.

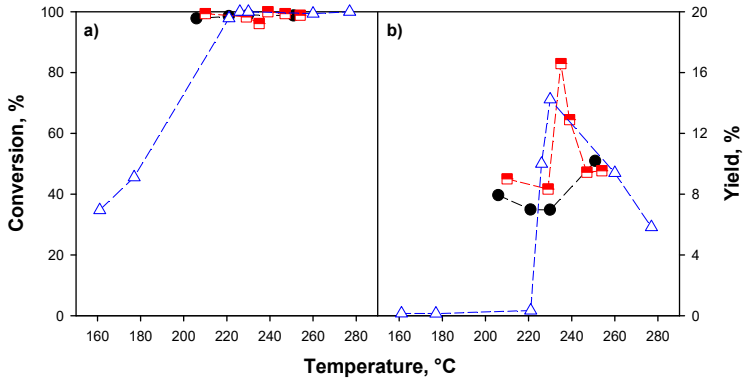

Figure 7. (**a**) Glycerol conversion, (**b**) yields to acrolein as a function of temperature at different contact times: 0.043 (full symbols), 0.057 (semi-filled symbols), 0.088 (open symbols) g·s·cm^{-3}; Gly/H_2O/O_2/N_2 = 2/41/6/51 vol. %.

2.2.2. Effect of the Support

The effect of the support has been studied at fixed contact time (τ = 0.057 g·s·cm^{-3}) and feed composition (Gly/H_2O/O_2/N_2 = 2/41/6/51 vol. %). As for VOP/Ti, acrylic acid, formic acid, and glycolic acid were detected. However, due to their very low amounts, the corresponding yields were not reported. In Figure 8, the glycerol conversion and the yields to acrolein, CO, CO_2, acetic acid, and coke obtained on the VOP/x catalysts are compared.

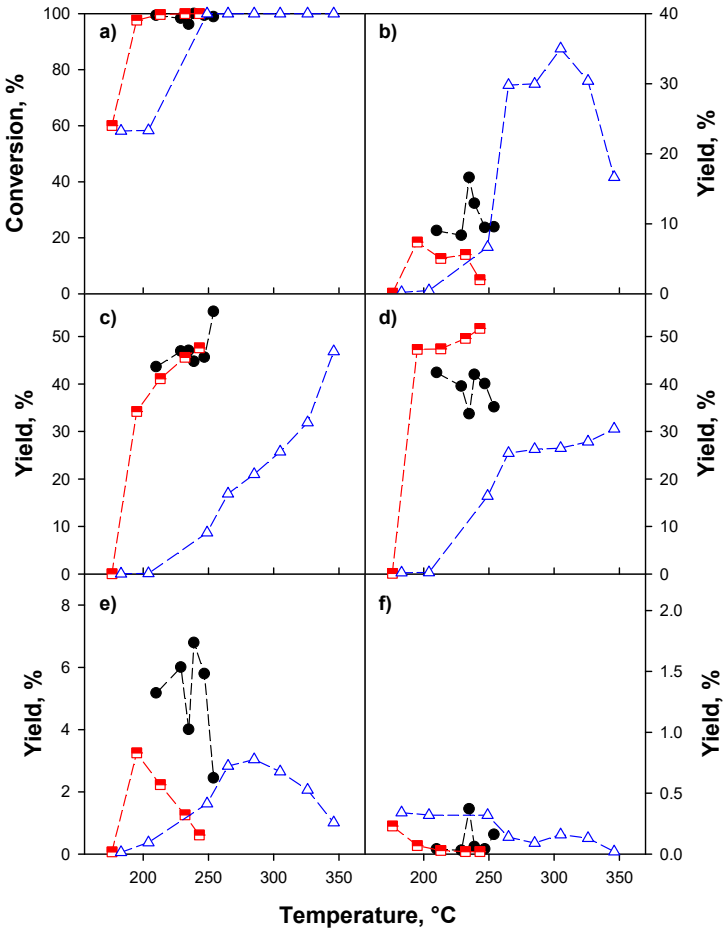

Figure 8. Glycerol conversion (**a**), yields to acrolein (**b**), to CO (**c**), to CO_2 (**d**), to acetic acid (**e**), and to coke (**f**) as a function of temperature on different VOP catalysts: VOP/Ti (full symbols), VOP/Zr (semi-filled symbols), VOP/Al (open symbols). τ = 0.057 g·s·cm^{-3}; Gly/H_2O/O_2/N_2 = 2/41/6/51 vol. %.

Glycerol conversion was about 60% on both VOP/Zr and VOP/Al at 180 °C. By increasing the temperature, glycerol conversion became quite complete at 200 °C for VOP/Zr, while higher temperatures were needed for VOP/Al (250 °C).

On VOP/Zr yields to acrolein and acetic acid show a maximum (7.4% and 3.3%, respectively) at about 200 °C. Their decrease is mainly compensated by a corresponding increase of the CO yield, in agreement with the results on VOP/Ti. Coke yield is very low in the whole temperature range, becoming entirely negligible above 200 °C. Carbon balance (not reported) is about 100% except at 180 °C, where it is about 40%. It is worth noting that no COx production was detected at this temperature. Thus, VOP/Zr could activate and convert glycerol into condensable species, but oxidation activity was negligible. As stated above, VOP/Al needs higher temperatures to convert glycerol fully. Interestingly, significant peak production of acrolein was obtained (35% yield) at about 300 °C, with about 30% yield in the temperature range 265–325 °C. Yield to acetic acid showed a maximum at 285 °C. The CO yield continuously increased while increasing the temperature, while the CO_2 yield showed a sharp increase between 200 and 265 °C, and then it increased moderately. Coke formation was higher than that obtained on the other samples, but it was still very low, being below 0.4% in the whole temperature range. Carbon balance is reported in Figure 9. It increased by increasing the temperature; however, it never reached 100%, with the highest value being 95%. This meant that (i) unknown products are produced in the whole temperature range (in low amounts starting from 300 °C) and (ii) the CO yield mainly increases due to the oxidation of the unknown species.

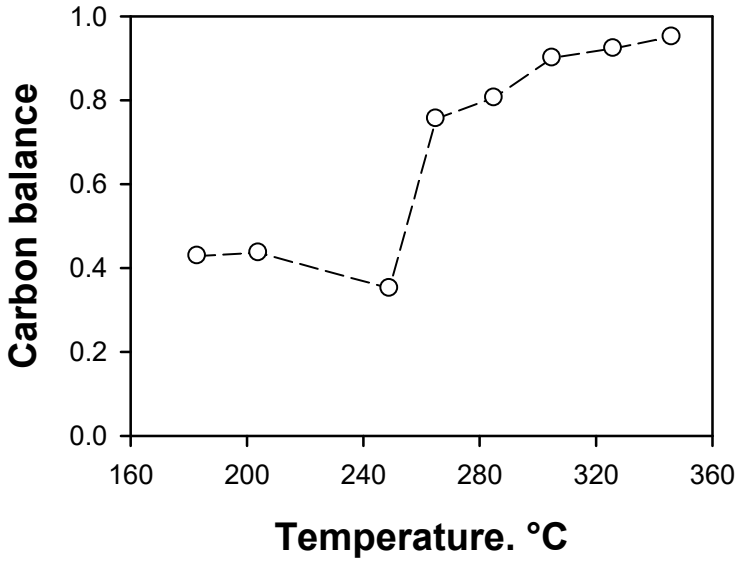

Figure 9. Carbon balance as a function of temperature on VOP/Al. τ = 0.057 g·s·cm^{-3}; Gly/H_2O/O_2/N_2 = 2/41/6/51 vol. %.

The behavior of the catalytic performance in terms of glycerol conversion and products distribution as a function of the reaction temperature is not directly related to the VOP amount. This result suggests the role of the support, as evidenced by NH_3-TPD characterization in terms of the acid sites distribution.

In this sample, the effect of oxygen concentration in the feed was studied (Figure 10) at 325 °C.

With respect to the reaction conditions reported above (O_2 = 6 vol. %), a slight oxygen decrease provided improved performance, with the yield to acrolein increasing to about 40%, while a decrease in the acrolein yield was found when increasing O_2 concentration, mainly due to acrolein oxidation.

In the presence of oxygen in the feed, glycerol conversion was 100%, while carbon balance was >90%, reaching 100% at 10 vol. % O_2 in the feed. On the contrary, in the absence of oxygen in the feed, glycerol conversion was incomplete, where the yield to acrolein decreased down to 15.7%, no CO_x production was detected (not reported) and the carbon balance declined to about 30%. Coke formation significantly increased, with coke yield being 1.5%. These results suggest that in the absence of

molecular oxygen, oxygenated compounds other than acrolein, acetic acid acrylic acid, glycolic acid, and formic acid, and high boiling point compounds, such as glycerol oligomers, acrolein oligomers, and aldol condensation products, are preferentially produced.

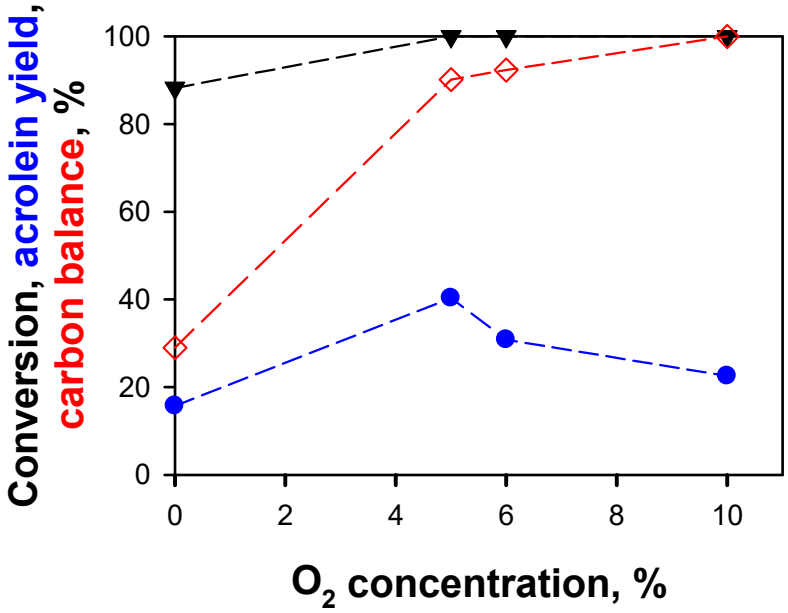

Figure 10. Conversion (▼), yield to acrolein (●), and carbon balance (◇) as a function of O_2 concentration in the feed on VOP/Al. T = 325 °C; τ = 0.057 g·s·cm^{-3}; Glycerol = 2 vol. %; H_2O = 41 vol. %; N_2 = balance.

3. Discussion

In this work, the dehydration of glycerol to acrolein over supported $VOPO_4$ (VOP) catalysts was studied. A theoretical VOP monolayer was supported on TiO_2, Al_2O_3, and ZrO_2; where deposition onto these supports guaranteed good active phase dispersion. All the samples show low coke formation in the presence of molecular oxygen in the feed, due to their redox properties. However, the higher the redox ability, the lower the acrolein yield due to the oxidation of the desired product to CO_x. Acrolein is the main condensable product, and low yields to acrylic acid, formic acid, acetic acid, and glycolic acid were measured. Unknown products are rarely detected; the corresponding reaction conditions are not interesting due to incomplete glycerol conversion and/or negligible acrolein production.

VOP supported onto alumina provided the best catalytic performances. Dehydration activity is related to the abundance of weak and medium acid sites, while its lowest redox activity preserves acrolein from oxidation. The catalysts investigated exhibit excellent resistance to coke formation, thereby suggesting it as a good candidate for the glycerol dehydration to acrolein.

Our best catalyst (VOP/Al) shows performance comparable to catalysts reported in the literature [27,28,31,37,58]. Better performances are reported with yields to acrolein in the range 70–90% [5,25,33,43,63]. However, deactivation phenomena due to coking are usually found. For instance, Katryniok et al. [64] defined a stable yield to acrolein equal to 60–65% in a two-zone fluidized bed as very promising.

Differently from the literature tested samples, the VOP/Al catalyst has shown very high resistance to coking. As a consequence, it is a good candidate for the glycerol dehydration to acrolein, provided that the active phase loading and the operating conditions are not optimized.

Future works will be devoted to the optimization of the active phase loading and the operating conditions to maximize the acrolein yield. Moreover, the effect of crude glycerol, containing several organic and inorganic impurities, will be investigated. Meanwhile, the presence of other organic

compounds can affect the reaction pathway, and the inorganic compounds (mainly alkali metal ions, such as Na^+ and K^+) can poison the catalyst by affecting the number and the strength of the acid sites.

4. Materials and Methods

4.1. Catalysts Preparation

Vanadyl orthophosphate, $VOPO_4 \cdot 2H_2O$ (VOP), was prepared as described in References [52,53]. γ-Al_2O_3 (CK-300 AKZO), anatase TiO_2 (Eurotitania), and ZrO_2 (prepared by conventional precipitation method [53]) were used as supports.

Each support was loaded with a VOP amount corresponding to a theoretical monolayer and, thus, depended on the support specific surface area, as reported in Table 1. The VOP was loaded onto the supports by the impregnation method, as described in Reference [53].

All these catalysts were indicated as VOP/M, where M was the metal ion of the oxide support.

4.2. Physico-Chemical Characterizations

The actual composition of the investigated samples was determined using inductively coupled plasma mass spectrometry (ICP-MS) analysis using an Agilent 7500CE instrument (Agilent, Santa Clara, CA, USA). Results showed differences with the nominal content within the experimental error (± 5%).

The specific surface areas (SSA) of supports and catalysts were measured by N_2 adsorption at 77 K with a Quantachrome Autosorb-1C instrument (Quantachrome, Boynton Beach, FL, USA) after degassing the samples at 150 °C for 1.5 h and calculated according to the Brunauer–Emmett–Teller (BET) method. No significant differences were detected between fresh and used samples.

X-ray diffraction (XRD) patterns of calcined catalysts were recorded using a Philips PW 1100 diffractometer (Philips, Eindhoven, Netherlands) with Ni-filtered Cu Kα radiation. Angular measurements (2θ) were accurate to 0.05°.

Temperature programmed desorption of ammonia (NH_3-TPD) were carried out using a Micromeritics Autochem II 2020 (Micromeritics, Norcross, GA, USA) equipped with a TC detector (Norcross, GA, USA). The samples (≈ 150 mg) were pre-treated in helium for 15 min at 450 °C, then saturated with a 5 vol. % NH_3/N_2 mixture for 1 h at 30 °C and washed in nitrogen for 0.5 h. The reactor was then heated at 10 °C/min up to 550 °C. NH_3-TPD profiles were deconvoluted using Origin software (OriginPro 2015 version) (OriginLab Corporation, Northampton, MA, USA, 2015). Three contributions were detected and assigned to weak, medium, and strong acid sites. NH_3-TPD tests were carried out on both the fresh and the used samples. No significant differences were detected.

Temperature programmed reduction in hydrogen (H_2-TPR) are reported in Reference [53], and here, they were used to discuss the relationship between catalytic activity and redox properties.

4.3. Catalytic Tests

Catalytic tests were conducted in a lab-scale test rig. The experimental apparatus was developed to carry out activity tests under stationary conditions, varying several operating parameters, such as temperature, reactant flow rates, and concentrations.

The flow rates of permanent gases (O_2 and N_2) were independently controlled using mass flow controllers (Brooks model SLA5850S), while a liquid 20 wt. % glycerol-water solution [5,18,31,64,65] was fed through a volumetric pump (KNF SIMDOS®02), vaporized using a heating tape, set at about 160 °C, and mixed with the permanent gases before entering the reactor. Pure glycerol (Sigma-Aldrich, purity ≥ 99.5%) was used as purchased. Crude glycerol from an alkali transesterification plant contains some impurities, such as methanol, soap, free fatty acids (FFAs), fatty acid methyl ester (FAMEs), glycerides. In addition, alkali metal ions (as Na^+ and K^+) are generally found in crude glycerol [66]; these alkali metals can poison the catalyst [66].

The catalyst (180–300 μm) was placed in a vertical quartz tube. The reaction temperature was set using a heating jacket (Tyco Thermal Controls) equipped with a PID controller. A K-type thermocouple was placed inside the reactor, thereby providing the reaction temperature.

Downstream the reactor, condensable species were separated from the gas mixture in three flasks in series placed in an ice bath. The collected liquid was analyzed off-line in a high-pressure liquid chromatography (HPLC) system (Agilent1100), provided with a refractive index detector (RID) and a diode Array type of UV/VIS Detector (DAD). Measurements were repeated three times, and the average values were used for the mass balance. However, values differed within the experimental error (±3%).

Incondensable species (CO, CO_2, O_2), dried by a $CaCl_2$ trap, were analyzed in a continuous analysis system (ABB AO2000), provided with a paramagnetic detector for O_2 measurement and a nondispersive infrared (NDIR) detector for CO and CO_2 measurements. The absolute uncertainty of the analyzer depends on the measurement range and corresponds to 50 ppm, 250 ppm, and 1000 ppm for CO, CO_2, and O_2, respectively. These values are much lower than the corresponding measurements during the reaction tests, thereby suggesting good reliability and accuracy of the measurements.

Gas-phase glycerol concentration was set at 2 vol. %, while oxygen concentration was in the range 0–10 vol. %. Nitrogen was used as a balance. The temperature was in the range 170–360 °C and the contact time in the range 0.04–0.09 $g \cdot s \cdot cm^{-3}$. It is worth noting that glycerol concentration was below its lower flammability limit (3 vol. %).

After each catalytic test, temperature-programmed oxidation (TPO) was carried out to (i) verify the formation of carbonaceous deposits onto the catalyst surface and (ii) clean the catalyst surface for the following catalytic test.

5. Conclusions

Supported vanadyl orthophosphate (VOP) were tested in the glycerol dehydration to acrolein. VOP supported onto γ-alumina showed the best performance, related to the highest amount of weak and medium acid sites. The oxygen co-feeding provides a good resistance to coking, which is, indeed, the main open issue of the catalytic systems for this reaction. The main by-products are CO and CO_2; while high selectivity towards acrolein is detected among the condensable products.

Catalytic performance is comparable to the performance of other catalytic systems but lower than that of the best catalysts. In this work, no reaction conditions nor active phase loading were optimized, suggesting that VOP supported onto γ-alumina are good candidates for glycerol dehydration to acrolein.

Author Contributions: Conceptualization, G.L. and A.D.B.; data curation, G.L. and G.R.; investigation, G.L., G.R. and A.D.B.; methodology, G.L., G.R., and A.D.B.; writing—original draft, G.L.; writing—review and editing, G.L., G.R., and A.D.B. All authors have read and agreed to the published version of the manuscript.

Funding: This research received no external funding.

Acknowledgments: The authors gratefully acknowledge Andrea Bizzarro for the BET analysis, Fernando Stanzione for the ICP-MS measurements and Luciano Cortese for the XRD measurements.

Conflicts of Interest: The authors declare no conflict of interest.

References

1. Ayoub, M.; Abdullah, A.Z. Critical review on the current scenario and significance of crude glycerol resulting from biodiesel industry towards more sustainable renewable energy industry. *Renew. Sustain. Energy Rev.* **2012**, *16*, 2671–2686. [CrossRef]
2. Mitrea, L.; Ranga, F.; Fetea, F.; Dulf, F.V.; Rusu, A.; Trif, M.; Vodnar, D.C. Biodiesel-Derived Glycerol Obtained from Renewable Biomass-A Suitable Substrate for the Growth of Candida zeylanoides Yeast Strain ATCC 20367. *Microorganisms* **2019**, *7*, 265. [CrossRef]
3. Vodnar, D.C.; Dulf, F.V.; Pop, O.L.; Socaciu, C. L (+)-lactic acid production by pellet-form Rhizopus oryzae NRRL 395 on biodiesel crude glycerol. *Microb. Cell Factories* **2013**, *12*, 92. [CrossRef] [PubMed]

4. Bindea, M.; Rusu, B.; Rusu, A.; Trif, M.; Leopold, L.; Dulf, F.V.; Vodnar, D.C. Valorification of crude glycerol for pure fractions of docosahexaenoic acid and β-carotene production by using Schizochytrium limacinum and Blakeslea trispora. *Microb. Cell Factories* **2018**, *17*, 97. [CrossRef] [PubMed]
5. Ren, X.; Zhang, F.; Sudhakar, M.; Wang, N.; Dai, J.; Liu, L. Gas-phase dehydration of glycerol to acrolein catalyzed by hybrid acid sites derived from transition metal hydrogen phosphate and meso-HZSM-5. *Catal. Today* **2019**, *332*, 20–27. [CrossRef]
6. Pagliaro, M.; Ciriminna, R.; Kimura, H.; Rossi, M.; Pina, C. Della Recent advances in the conversion of bioglycerol into value-added products. *Eur. J. Lipid Sci. Technol.* **2009**, *111*, 788–799. [CrossRef]
7. Dharmadi, Y.; Murarka, A.; Gonzalez, R. Anaerobic fermentation of glycerol byEscherichia coli: A new platform for metabolic engineering. *Biotechnol. Bioeng.* **2006**, *94*, 821–829. [CrossRef]
8. Deckwer, W.-D. Microbial conversion of glycerol to 1,3-propanediol. *FEMS Microbiol. Rev.* **1995**, *16*, 143–149. [CrossRef]
9. Anuar, M.R.; Abdullah, A.Z. Challenges in biodiesel industry with regards to feedstock, environmental, social and sustainability issues: A critical review. *Renew. Sustain. Energy Rev.* **2016**, *58*, 208–223. [CrossRef]
10. Stelmachowski, M. Utilization of glycerol, a by-product of the transestrification process of vegetable oils: A review. *Ecol. Chem. Eng. S* **2011**, *18*, 9–30.
11. Anitha, M.; Kamarudin, S.K.; Kofli, N.T. The potential of glycerol as a value-added commodity. *Chem. Eng. J.* **2016**, *295*, 119–130. [CrossRef]
12. Li, C.; He, B.; Ling, Y.; Tsang, C.-W.; Liang, C. Glycerol hydrogenolysis to n-propanol over Zr-Al composite oxide-supported Pt catalysts. *Chin. J. Catal.* **2018**, *39*, 1121–1128. [CrossRef]
13. Ma, Y.; Wang, Y.-M.; Morgan, P.J.; Jackson, R.E.; Liu, X.; Saunders, G.C.; Lorenzini, F.; Marr, A.C. Designing effective homogeneous catalysis for glycerol valorisation: Selective synthesis of a value-added aldehyde from 1,3-propanediol via hydrogen transfer catalysed by a highly recyclable, fluorinated Cp*Ir(NHC) catalyst. *Catal. Today* **2018**, *307*, 248–259. [CrossRef]
14. Nakagawa, Y.; Tamura, M.; Tomishige, K. Perspective on catalyst development for glycerol reduction to C3 chemicals with molecular hydrogen. *Res. Chem. Intermed.* **2018**, *44*, 3879–3903. [CrossRef]
15. Wu, Z.; Zhang, M.; Yao, Y.; Wang, J.; Wang, D.; Zhang, M.; Li, Y. One-pot catalytic production of 1,3-propanediol and γ-valerolactone from glycerol and levulinic acid. *Catal. Today* **2018**, *302*, 217–226. [CrossRef]
16. Yfanti, V.-L.; Ipsakis, D.; Lemonidou, A.A. Kinetic study of liquid phase glycerol hydrodeoxygenation under inert conditions over a Cu-based catalyst. *React. Chem. Eng.* **2018**, *3*, 559–571. [CrossRef]
17. De Abreu, T.H.; Meyer, C.I.; Padró, C.; Martins, L. Acidic V-MCM-41 catalysts for the liquid-phase ketalization of glycerol with acetone. *Microporous Mesoporous Mater.* **2019**, *273*, 219–225. [CrossRef]
18. Basile, F.; Cavani, F.; Chieregato, A.; Concepción, P.; Liosi, G.; López Nieto, J.M.; Soriano, M.D.; Trevisanut, C. Glycerol oxidehydration into acrolein and acrylic acid over W/V/Nb bronzes with hexagonal structure. *DGMK Tag.* **2012**, *2012*, 189–193.
19. Bozga, E.; Plesu, V.; Bozga, G. Conversion of Glycerol to Propanediol and Acrolein by Heterogeneous Catalysis. *Rev. Chim. Bucharest* **2011**, *62*, 646–654.
20. Célerier, S.; Morisset, S.; Batonneau-Gener, I.; Belin, T.; Younes, K.; Batiot-Dupeyrat, C. Glycerol dehydration to hydroxyacetone in gas phase over copper supported on magnesium oxide (hydroxide) fluoride catalysts. *Appl. Catal. A Gen.* **2018**, *557*, 135–144. [CrossRef]
21. Christy, S.; Noschese, A.; Lomelí-Rodriguez, M.; Greeves, N.; Lopez-Sanchez, J.A. Recent progress in the synthesis and applications of glycerol carbonate. *Curr. Opin. Green Sustain. Chem.* **2018**, *14*, 99–107. [CrossRef]
22. Deleplanque, J.; Dubois, J.L.; Devaux, J.F.; Ueda, W. Production of acrolein and acrylic acid through dehydration and oxydehydration of glycerol with mixed oxide catalysts. *Catal. Today* **2010**, *157*, 351–358. [CrossRef]
23. Gabrysch, T.; Peng, B.; Bunea, S.; Dyker, G.; Muhler, M. The Role of Metallic Copper in the Selective Hydrodeoxygenation of Glycerol to 1,2-Propanediol over Cu/ZrO_2. *ChemCatChem* **2018**, *10*, 1344–1350. [CrossRef]
24. Liu, L.; Ye, X.P.; Bozell, J.J. A Comparative Review of Petroleum-Based and Bio-Based Acrolein Production. *ChemSusChem* **2012**, *5*, 1162–1180. [CrossRef]
25. Zhang, F.; Ren, X.; Huang, H.; Huang, J.; Sudhakar, M.; Liu, L. High-performance phosphate supported on HZSM-5 catalyst for dehydration of glycerol to acrolein. *Chin. J. Chem. Eng.* **2018**, *26*, 1031–1040. [CrossRef]

26. Ding, J.; Ma, T.; Shao, R.; Xu, W.; Wang, P.; Song, X.; Guan, R.; Yeung, K.; Han, W. Gas phase dehydration of glycerol to acrolein on an amino siloxane-functionalized MCM-41 supported Wells–Dawson type $H_6P_2W_{18}O_{62}$ catalyst. *New. J. Chem.* **2018**, *42*, 14271–14280. [CrossRef]
27. Possato, L.G.; Chaves, T.F.; Cassinelli, W.H.; Pulcinelli, S.H.; Santilli, C.V.; Martins, L. The multiple benefits of glycerol conversion to acrolein and acrylic acid catalyzed by vanadium oxides supported on micro-mesoporous MFI zeolites. *Catal. Today* **2017**, *289*, 20–28. [CrossRef]
28. Cecilia, J.A.; García-Sancho, C.; Mérida-Robles, J.M.; Santamaría González, J.; Moreno-Tost, R.; Maireles-Torres, P. WO3 supported on Zr doped mesoporous SBA-15 silica for glycerol dehydration to acrolein. *Appl. Catal. A Gen.* **2016**, *516*, 30–40. [CrossRef]
29. Diallo, M.M.; Laforge, S.; Pouilloux, Y.; Mijoin, J. Highly Efficient Dehydration of Glycerol to Acrolein Over Isomorphously Substituted Fe-MFI Zeolites. *Catal. Lett.* **2018**, *148*, 2283–2303. [CrossRef]
30. Beerthuis, R.; Huang, L.; Shiju, N.R.; Rothenberg, G.; Shen, W.; Xu, H. Facile Synthesis of a Novel Hierarchical ZSM-5 Zeolite: A Stable Acid Catalyst for Dehydrating Glycerol to Acrolein. *ChemCatChem* **2018**, *10*, 211–221. [CrossRef]
31. Han, Q.; Ge, J.; Yang, Y.; Liu, B. Nickel substituted tungstophosphoric acid supported on Y-ASA composites as catalysts for the dehydration of gas-phase glycerol to acrolein. *React. Kinet. Mech. Catal.* **2019**, *127*, 331–343. [CrossRef]
32. Ding, J.; Yan, C.; Ma, T.; Shao, R.; Xu, W.; Wang, P. Gas phase dehydration of glycerol to acrolein over $NaHSO_4$@Zr-MCM-41 catalyst. *Can. J. Chem. Eng.* **2019**, *97*, 1152–1159. [CrossRef]
33. Kraleva, E.; Atia, H. Keggin-type heteropolyacids supported on sol–gel oxides as catalysts for the dehydration of glycerol to acrolein. *React. Kinet. Mech. Catal.* **2019**, *126*, 103–117. [CrossRef]
34. Shan, J.; Li, Z.; Zhu, S.; Liu, H.; Li, J.; Wang, J.; Fan, W. Nanosheet MFI Zeolites for Gas Phase Glycerol Dehydration to Acrolein. *Catalysts* **2019**, *9*, 121. [CrossRef]
35. Lauriol-Garbey, P.; Millet, J.M.M.; Loridant, S.; Bellire-Baca, V.; Rey, P. New efficient and long-life catalyst for gas-phase glycerol dehydration to acrolein. *J. Catal.* **2011**, *281*, 362–370. [CrossRef]
36. Ding, J.; Ma, T.; Cui, M.; Shao, R.; Guan, R.; Wang, P. Gas phase dehydration of glycerol to acrolein over Cs2.5H0.5PW12O40/Zr-MCM-41 catalysts prepared by supercritical impregnation. *Mol. Catal.* **2018**, *461*, 1–9. [CrossRef]
37. Srinivasa Rao, G.; Hussain, S.; Chary, K.V.R. Porous zirconium phosphate solid acid catalysts with variable Zr/P ratio for gas phase glycerol dehydration to acrolein. In *Materials Today: Proceedings*; Elsevier: Amsterdam, The Netherlands, 2018; pp. 25773–25781.
38. Ding, J.; Ma, T.; Yun, Z.; Shao, R. Heteropolyacid (H3PW12O40) supported MCM-41: An effective solid acid catalyst for the dehydration of glycerol to acrolein. *J. Wuhan Univ. Technol. Mater. Sci. Ed.* **2017**, *32*, 1511–1516. [CrossRef]
39. Wang, F.; Dubois, J.L.; Ueda, W. Catalytic dehydration of glycerol over vanadium phosphate oxides in the presence of molecular oxygen. *J. Catal.* **2009**, *268*, 260–267. [CrossRef]
40. Talebian-Kiakalaieh, A.; Amin, N.A.S.; Zakaria, Z.Y. Gas phase selective conversion of glycerol to acrolein over supported silicotungstic acid catalyst. *J. Ind. Eng. Chem.* **2016**, *34*, 300–312. [CrossRef]
41. Huang, L.; Qin, F.; Huang, Z.; Zhuang, Y.; Ma, J.; Xu, H.; Shen, W. Metal–Organic Framework Mediated Synthesis of Small-Sized γ-Alumina as a Highly Active Catalyst for the Dehydration of Glycerol to Acrolein. *ChemCatChem* **2018**, *10*, 381–386. [CrossRef]
42. Ma, T.; Yun, Z.; Xu, W.; Chen, L.; Li, L.; Ding, J.; Shao, R. *Pd-H3PW12O40/Zr-MCM-41: An Efficient Catalyst for the Sustainable Dehydration of Glycerol to Acrolein*; Elsevier: Amsterdam, The Netherlands, 2016.
43. Nadji, L.; Massó, A.; Delgado, D.; Issaadi, R.; Rodriguez-Aguado, E.; Rodriguez-Castellón, E.; Nieto, J.M.L. Gas phase dehydration of glycerol to acrolein over WO_3-based catalysts prepared by non-hydrolytic sol–gel synthesis. *RSC Adv.* **2018**, *8*, 13344–13352. [CrossRef]
44. Ma, T.; Ding, J.; Shao, R.; Yun, Z. Catalytic conversion of glycerol to acrolein over MCM-41 by the grafting of phosphorus species. *Can. J. Chem. Eng.* **2016**, *94*, 924–930. [CrossRef]
45. Lauriol-Garbey, P.; Loridant, S.; Bellière-Baca, V.; Rey, P.; Millet, J.M.M. Gas phase dehydration of glycerol to acrolein over WO_3/ZrO_2 catalysts: Improvement of selectivity and stability by doping with SiO_2. *Catal. Commun.* **2011**, *16*, 170–174. [CrossRef]

46. Znaiguia, R.; Brandhorst, L.; Christin, N.; Bellière Baca, V.; Rey, P.; Millet, J.M.M.; Loridant, S. Toward longer life catalysts for dehydration of glycerol to acrolein. *Microporous Mesoporous Mater.* **2014**, *196*, 97–103. [CrossRef]
47. Katryniok, B.; Paul, S.; Capron, M.; Dumeignil, F. Towards the sustainable production of acrolein by glycerol dehydration. *ChemSusChem* **2009**, *2*, 719–730. [CrossRef]
48. Jiang, X.C.; Zhou, C.H.; Tesser, R.; Di Serio, M.; Tong, D.S.; Zhang, J.R. Coking of Catalysts in Catalytic Glycerol Dehydration to Acrolein. *Ind. Eng. Chem. Res.* **2018**, *57*, 10736–10753. [CrossRef]
49. Dos Santos, M.B.; Andrade, H.M.C.; Mascarenhas, A.J.S. Reduced coke formation during the gas phase oxidative dehydration of glycerol over ferrierite zeolites synthesized in fluoride medium. *Microporous Mesoporous Mater.* **2016**, *223*, 105–113. [CrossRef]
50. Park, H.; Yun, Y.S.; Kim, T.Y.; Lee, K.R.; Baek, J.; Yi, J. Kinetics of the dehydration of glycerol over acid catalysts with an investigation of deactivation mechanism by coke. *Appl. Catal. B Environ.* **2015**, *176–177*, 1–10. [CrossRef]
51. Talebian-Kiakalaieh, A.; Amin, N.A.S. Coke-tolerant SiW20-Al/Zr10 catalyst for glycerol dehydration to acrolein. *Cuihua Xuebao/Chin. J. Catal.* **2017**, *38*, 1697–1710. [CrossRef]
52. Casaletto, M.P.; Lisi, L.; Mattogno, G.; Patrono, P.; Ruoppolo, G.; Russo, G. Oxidative dehydrogenation of ethane on γ-Al_2O_3 supported vanadyl and iron vanadyl phosphates: Physico-chemical characterisation and catalytic activity. *Appl. Catal. A Gen.* **2002**, *226*, 41–48. [CrossRef]
53. Casaletto, M.P.; Landi, G.; Lisi, L.; Patrono, P.; Pinzari, F. Effect of the support on the catalytic properties of vanadyl phosphate in the oxidative dehydrogenation of propane. *J. Mol. Catal. A Chem.* **2010**, *329*, 50–56. [CrossRef]
54. Cavani, F.; Luciani, S.; Esposti, E.D.; Cortelli, C.; Leanza, R. Surface Dynamics of A Vanadyl Pyrophosphate Catalyst for *n*-Butane Oxidation to Maleic Anhydride: An In Situ Raman and Reactivity Study of the Effect of the P/V Atomic Ratio. *Chem. A Eur. J.* **2010**, *16*, 1646–1655. [CrossRef] [PubMed]
55. Caldarelli, A.; Cavani, F.; Folco, F.; Luciani, S.; Cortelli, C.; Leanza, R. The design of a new ZrO_2-supported V/P/O catalyst for n-butane oxidation to maleic anhydride: The build-up of the active phase during thermal treatment. In *Catalysis Today*; Elsevier: Amsterdam, The Netherlands, 2010; pp. 204–210.
56. Chieregato, A.; Bandinelli, C.; Concepción, P.; Soriano, M.D.; Puzzo, F.; Basile, F.; Cavani, F.; Nieto, J.M.L. Structure-Reactivity Correlations in Vanadium-Containing Catalysts for One-Pot Glycerol Oxidehydration to Acrylic Acid. *ChemSusChem* **2017**, *10*, 234–244. [CrossRef] [PubMed]
57. Landi, G.; Lisi, L.; Volta, J.C. Oxidation of propane to acrylic acid over vanadyl pyrophosphate: Modifications of the structural and acid properties during the precursor activation and their relationship with catalytic performances. *J. Mol. Catal. A Chem.* **2004**, *222*, 175–181. [CrossRef]
58. Pethan Rajan, N.; Rao, G.S.; Pavankumar, V.; Chary, K.V.R. Vapour phase dehydration of glycerol over VPO catalyst supported on zirconium phosphate. *Catal. Sci. Technol.* **2014**, *4*, 81–92. [CrossRef]
59. Casaletto, M.P.; Lisi, L.; Mattogno, G.; Patrono, P.; Ruoppolo, G. Effect of the support on the surface composition of vanadium phosphate catalysts in the oxidative dehydrogenation of ethane. In *Surface and Interface Analysis*; John Wiley & Sons, Ltd.: Hoboken, NJ, USA, 2004; pp. 737–740.
60. García-Sancho, C.; Cecilia, J.A.; Mérida-Robles, J.M.; Santamaría González, J.; Moreno-Tost, R.; Infantes-Molina, A.; Maireles-Torres, P. Effect of the treatment with H3PO4on the catalytic activity of Nb2O5supported on Zr-doped mesoporous silica catalyst. Case study: Glycerol dehydration. *Appl. Catal. B Environ.* **2018**, *221*, 158–168. [CrossRef]
61. Vieira, L.H.; Carvalho, K.T.G.; Urquieta-González, E.A.; Pulcinelli, S.H.; Santilli, C.V.; Martins, L. Effects of crystal size, acidity, and synthesis procedure on the catalytic performance of gallium and aluminum MFI zeolites in glycerol dehydration. *J. Mol. Catal. A Chem.* **2016**, *422*, 148–157. [CrossRef]
62. Wang, F.; Dubois, J.L.; Ueda, W. Catalytic performance of vanadium pyrophosphate oxides (VPO) in the oxidative dehydration of glycerol. *Appl. Catal. A Gen.* **2010**, *376*, 25–32. [CrossRef]
63. Xie, Q.; Li, S.; Gong, R.; Zheng, G.; Wang, Y.; Xu, P.; Duan, Y.; Yu, S.; Lu, M.; Ji, W.; et al. Microwave-assisted catalytic dehydration of glycerol for sustainable production of acrolein over a microwave absorbing catalyst. *Appl. Catal. B Environ.* **2019**, *243*, 455–462. [CrossRef]
64. Katryniok, B.; Meléndez, R.; Bellière-Baca, V.; Rey, P.; Dumeignil, F.; Fatah, N.; Paul, S. Catalytic Dehydration of Glycerol to Acrolein in a Two-Zone Fluidized Bed Reactor. *Front. Chem.* **2019**, *7*, 127. [CrossRef]

65. Lauriol-Garbey, P.; Postole, G.; Loridant, S.; Auroux, A.; Belliere-Baca, V.; Rey, P.; Millet, J.M.M. Acid-base properties of niobium-zirconium mixed oxide catalysts for glycerol dehydration by calorimetric and catalytic investigation. *Appl. Catal. B Environ.* **2011**, *106*, 94–102. [CrossRef]
66. Lu, Q.; Liu, R.; Xia, G. Sequential Dehydration and Oxidation of Biodiesel-derived Crude Glycerol into Acrylic Acid. *Russ. J. Appl. Chem.* **2018**, *91*, 235–244. [CrossRef]